Journal of the European Ceramic Society 35 (2015) 4321–4325

Contents lists available at www.sciencedirect.com

Journal of the European Ceramic Society

journal homepage: www.elsevier.com/locate/jeurceramsoc

Short communication

Quantification of crystalline texture in ferroelectric materials by polarized Raman spectroscopy using Reverse Monte Carlo modelling

Sören Röhrig[a,b], Clemens Krautgasser[a,b], Raul Bermejo[b], Jacob L. Jones[c], Peter Supancic[a,b], Marco Deluca[a,b,*]

[a] Materials Center Leoben Forschung GmbH, Roseggerstraße 12, 8700 Leoben, Austria
[b] Institut für Struktur- und Funktionskeramik, Montanuniversitaet Leoben, Peter Tunner Straße 5, 8700 Leoben, Austria
[c] Department of Materials Science & Engineering, North Carolina State University, NC 27695 Raleigh, USA

ARTICLE INFO

Article history:
Received 2 July 2015
Received in revised form 27 July 2015
Accepted 1 August 2015
Available online 15 August 2015

Keywords:
Ferroelectric domains
Ferroelasticity
Domain texture
Orientation distribution function
Reverse Monte Carlo
Raman spectroscopy

ABSTRACT

A Reverse Monte Carlo (RMC) model for the quantification of the crystalline texture in ferroelectric/ferroelastic ceramics based on polarized Raman spectroscopy (PRS) measurements has been developed and compared with analytical fitting approaches. We demonstrate, also by validation with PRS experiments on ferroelectric samples with different texture degrees, that the RMC model is more effective in reproducing physical features, including the saturated domain state. The versatility of the RMC model opens new possibilities for texture studies by PRS, and can be in principle applied to any kind of Raman-active material.

Texture in ceramic materials can be tailored to improve both mechanical and functional properties [1,2]. In ferroelectric ceramics, a form of texturing can be associated with the preferred orientation of polarized regions, called ferroelectric domains. These are induced by spontaneous polarization, and can be altered by electric field (poling), mechanical stress and/or temperature by domain switching. This affects the remanent states and lastly the piezoelectric properties of the material [3]. A material commonly used for sensor and actuator applications - where the performance is related to the degree of domain texture—is lead zirconate titanate (PZT) [3]. Domain switching is always constrained by the orientation of the grains in which they are contained. Thus, if the grains are initially randomly oriented, there is a limit on the achievable domain orientation [4,5]. Consequently, the electro-mechanical coupling can be enhanced if the grains are preferentially oriented [1,6]. Hence, it is very important in piezoceramics to investigate the orientation distribution of domains in order to understand and improve factors influencing reliability and performance.

Polarized Raman spectroscopy (PRS) has been extensively used to detect texture in crystalline solids and polymers [7–11]. Compared to other methods such as X-ray diffraction [12,13] and electron back-scattered diffraction [14], PRS has the advantage of achieving micrometre spatial resolution with laboratory-scale equipment, requiring very little sample preparation. In the PRS analysis, the intensity of selected Raman modes varies sinusoidally in dependence of the angle between laser polarization and the sample preferential orientation. Hence, information on the local texture can be obtained [9,10,15–17]. In the past literature, the reconstruction of a texture orientation distribution function (ODF) of ferroelectric domains from PRS data has been based on analytical functions [8,18]. These approaches have the general drawback of not considering that the domain axis is constrained to the underlying grain orientation, which is generally random in ceramics, nor that the switching capability of domains is restricted by the symmetry of the crystalline unit cell.

The maximum theoretically achievable domain orientation in a uniaxially poled tetragonal ferroelectric polycrystal can be described analytically by a piecewise function [19] (cf. Fig. 1, straight line). This ODF can be modelled with an analytical approach based on spherical harmonics [8]. Given the assumption of uniaxial symmetry (valid in poled ferroelectrics), two terms of the series are sufficient to represent the ODF [8,18]:

$$\mathrm{ODF}(\theta) \propto 1 + \lambda_2 P_2(\cos\theta) + \lambda_4 P_4(\cos\theta) \quad (1)$$

* Corresponding author.
E-mail address: marco.deluca@mcl.at (M. Deluca).

http://dx.doi.org/10.1016/j.jeurceramsoc.2015.08.003

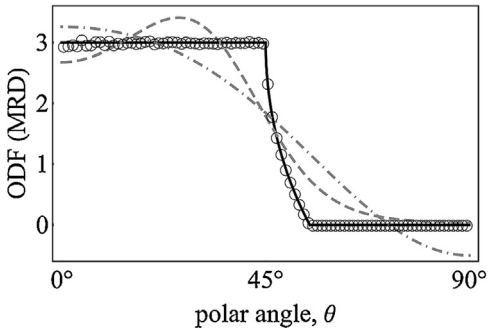

Fig. 1. Texture ODF of ferroelastic domains in a tetragonal saturated poled material shown as a multiple of a random distribution (MRD). Straight, black line: Saturated configuration (after Jones [5] and Li [13]); Dot-dashed, grey line: best fit with Spherical Harmonics (Eq. (1); $\lambda_2 = 2.683$ and $\lambda_4 = -0.4252$); dashed, grey line: best fit with exponential approach (Eq. (2); $\lambda_2 = -3.42$ and $\lambda_4 = 1.536$) , empty circles: best fit with 2×10^5 discrete domains, binned in 1° intervals.

where θ is the polar angle, P_2 and P_4 are the second and fourth Legendre polynomials, respectively, λ_2 and λ_4 are fitting parameters. This approach is not capable of fitting the saturated curve reported in Fig. 1 (cf. grey dot-dashed line). In particular, negative values of the ODF are obtained close to the axis perpendicular to poling. In an attempt to avoid this unphysical issue, an exponential function was proposed [18]:

$$\mathrm{ODF}(\theta) \propto \exp\{-[\lambda_2 P_2(\cos\theta) + \lambda_4 P_4(\cos\theta)]\} \quad (2)$$

The curve is shown as a dashed grey line in Fig. 1; clearly, this approach also overestimates the saturated ODF (i.e. the maximum achievable orientation in a tetragonal material), thus leading to unphysical results.

An alternative approach involving discretization of the ODF into orientation bins can overcome these limitations. In Fig. 1 the black dots represent a fit performed using a discrete ensemble of 2×10^5 domains, binned in 1° interval (analogous to Jones et al. [5]). Clearly, this approach is the most versatile as it fits perfectly the saturated ODF and prevents obtaining inconsistencies and unphysical results. In this work, we used the latter approach for texture representation and developed a Reverse Monte Carlo (RMC) model to extract a discrete ODF from the treatment of PRS experimental data. To validate the model, PRS results obtained from three PZT samples with different domain texture were employed, comparing the results of RMC with an analytical approach. It is shown that RMC simulation can provide a physically coherent ODF starting from Raman data, including the constraints posed by grain orientation and crystal symmetry, thus allowing a limited number of domain switching orientations.

Commercial soft PZT samples (with composition close to the morphotropic phase boundary but within the tetragonal phase range) were supplied by the company EPCOS OHG (Deutschlandsberg, Austria). Three bar-shaped specimens ($10 \times 4 \times 2.5\,\mathrm{mm}^3$) were prepared: (i) unpoled, (ii) poled, and (iii) mechanically compressed, to produce different domain configurations. Further details on sample preparation are given elsewhere [20]. Poling was performed longitudinally with an electric field of 2 kV/mm. Mechanically compressed samples were initially poled, then heated up to 400 °C (above the Curie temperature, T_c) and lastly mechanically loaded up to 25 MPa on the longitudinal axis, holding the compressive load during cooling down to room temperature.

The macroscopic textured state of the three samples was qualitatively assessed calculating the crack growth resistance (CGR), which in ferroelastic materials correlates with the underlying domain texture [20,21], along relevant directions in the sample coordinate system. A series of Vickers indentations was introduced in the samples, the indent corners being oriented parallel or perpendicular with respect to the longitudinal axis, respectively. From the lengths of the corresponding indentation cracks in parallel (a^{II}) and perpendicular ($a^{\perp}$) direction, the CGR was evaluated (K_R^{II} and $K_R^{\perp}$, respectively) according to the method described in [20,22,23] (cf. Table 1). In unpoled samples, the CGR is isotropic in both directions. In poled and compressed samples, due to ferroelastic domain switching, it is anisotropic and dependent on the preferential texture direction (i.e. higher CGR parallel to texture main axis). These results confirm the presence of a macroscopic ferroelectric domain texture both in poled and in compressed samples.

Table 1
Crack length and CGR in differently prepared samples.

Sample	$a^{II}/(\mu m)$	$a^{\perp}/(\mu m)$	$K_R^{\mathrm{II}}/(\mathrm{MPa\,m^{1/2}})$	$K_R^{\perp}/(\mathrm{MPa\,m^{1/2}})$
unpoled	192 ± 3	194 ± 2	1.15 ± 0.03	1.13 ± 0.02
poled	159 ± 4	272 ± 5	1.52 ± 0.06	0.68 ± 0.02
compressed	243 ± 5	133 ± 8	0.81 ± 0.02	2.08 ± 0.08

PRS experiments were performed using a LabRam HR-800 (Horiba/Jobin-Yvon, Villeneuve d'Ascq, France) with 514.5 nm laser excitation, focused on the sample's surface via a 100x long-working distance microscope lens (Olympus, Tokyo, Japan). Further details on the experimental settings of the Raman equipment are described in Ref. [11]. Texture measurements were performed with a rotating microscope stage, collecting spectra from 0° to 180° every 10°

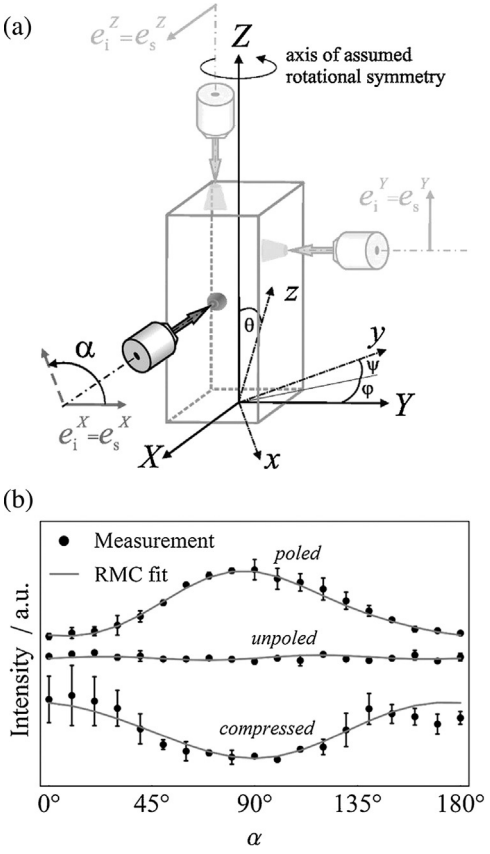

Fig. 2. (a) Polarization settings used for Raman experiment and RMC model. Euler angles (φ, θ and ψ) describe sequential rotation (intrinsic *y*-convention: *z*, *y'*, *z"*) between the sample coordinate system (X, Y, Z) and the crystallite coordinate system (*x*, *y*, *z*). Three Raman observation directions are displayed, each one with the incident/scattered polarization direction indicated for (straight arrow). Since only illumination along the X direction was used in the present work, the other two directions are represented with faded colour. The Z-axis (longitudinal axis) is the rotational axis of the samples' texture. (b) Angular dependent, normalized Raman intensities for the investigated samples, measured on the YZ-plane; the standard deviation is based on two measurements. The solid lines report the fitting performed with the RMC model.

of rotation. The angle α between laser polarization and sample orientation was varied (cf. Fig. 2a). On each sample, two points were measured on the YZ plane (with X as direction of observation). Raman spectra were normalized and then imported into a commercial software environment (Labspec 4.02, Horiba/Jobin-Yvon). Deconvolution was performed with Gaussian–Lorentzian peak functions after subtracting a linear baseline. The angular dependence of the parallel polarized intensity of the Raman mode of A_1 symmetry at ~220 cm^{-1} [16] was extracted, averaged and normalized (Fig. 2b, cf. the measured points). The unpoled sample shows no intensity angular dependence, whereas the poled and the compressed ones display sinusoidal intensity dependence with 180° periodicity, the phase being shifted by 90°. This preliminary finding suggests no texture in the unpoled sample, and the presence of texture (with preferential orientation shifted by 90°) in the other ones, in agreement with the CGR results.

The texture ODF was determined by fitting the angular dependent data from Fig. 2b using an RMC approach [24,25]. Within this model, the orientation of a domain is represented by its principal axis system, a set of three orthogonal vectors (triad). The *z*-axis determines the polarization vector of the corresponding domain. Euler angles (i.e. ϕ, θ and ψ) are used to describe the orientation of each triad with respect to the sample coordinate system (cf. Fig. 2a). For a given distribution based on *n* triads, the calculated polarized Raman intensity $\left(I^j_{\mathrm{sim}}\right)$ of a given Raman mode can be written with respect to the rotation angle α, assuming parallel polarization and backscattering configuration [15]:

$$I^j_{\mathrm{sim}}(\alpha) \propto \sum_k^n \left| e^j_s(\alpha)\, \Re^{\mathrm{rot}}_k e^j_i(\alpha) \right|^2 \tag{3}$$

where $e^j_i = e^j_s$ represent the incident and the scattered polarization vector, respectively; *j* indicates the propagation direction of the laser beam with respect to the sample coordinate system (cf. Fig. 2a) and $\Re^{\mathrm{rot}}_k$ is the Raman tensor of the selected mode for each triad represented in the sample's coordinate system. For an A_1 mode in the tetragonal (*4 mm*) symmetry, the Raman tensor in its principal axes is:

$$\Re = \begin{pmatrix} a & 0 & 0 \\ 0 & a & 0 \\ 0 & 0 & b \end{pmatrix} \tag{4}$$

In PZT, the ratio $\frac{b}{a} = -2.15$ according to Raman measurements on quasi-single-crystalline samples [26]. For each triad, the orientation of the Raman tensor with respect to the laboratory system has to be expressed with a second order tensor transformation [27]. Due to the rotational symmetry of the Raman tensor in Eq. (4), there is no dependence on ψ.

To account for the effects of the numerical aperture (NA) of the microscope objective and the refractive index of the sample ($n_S \approx 2.7$ for PZT for the used radiation wavelength [28]), a more accurate version of Eq. (3) was used here [17]:

$$I^j_{\mathrm{sim}}(\alpha) = \sum_k^n \int_0^{2\pi} \int_0^{\gamma_m} \left| \left(T(\vartheta, \gamma)\, e^j_i(\alpha) \right) \Re^{\mathrm{rot}}_k e^j_s(\alpha) \right|^2 \sin\gamma d\gamma d\vartheta \tag{5}$$

where *T* is the "microscope-objective transfer matrix" [17], and γ_m is half the aperture angle of the radiation cone probing the sample $\left(\text{i.e. } \sin\gamma_m = \frac{\mathrm{NA}}{n_S}\right)$. For normalization purposes we used

$$\hat{I}^j_{\mathrm{sim}}(\alpha) = \frac{I^j_{\mathrm{sim}}(\alpha)}{\int_{0^\circ}^{180^\circ} I^j_{\mathrm{sim}}(\alpha)\, d\alpha} \tag{6}$$

The RMC fitting procedure starts with randomly oriented triads. Stepwise, the *z*-axis (i.e. the polar axis) of a randomly accessed triad is reoriented randomly by 90° or 180° steps, which yields in total six possible orientations per triad.[1] Note: the change of *x*, *y* axes is not tracked since they have no impact on the Raman signal (due to the cylindrical symmetry of the Raman tensor). This constraint on the possible reorientations is posed by the tetragonal symmetry, and has the consequence that only a few new orientations are possible with respect to the original position of each triad. This mimics the constraint derived from the (random) grain orientation and from unit cell symmetry, which guarantees a physically coherent distribution.

After the switching of one triad, a new normalized angular dependent Raman intensity $\hat{I}^j_{\mathrm{sim}}$ (from Eqs. (5), (6)) is calculated and compared to the measured results, using a standard χ^2 test [25]:

$$\chi^2 = \frac{\sum_j \sum_{\alpha_i} \left(\hat{I}^j_{\mathrm{meas}}(\alpha_i) - \hat{I}^j_{\mathrm{sim}}(\alpha_i) \right)^2}{\left(\hat{\sigma}^j_{\mathrm{meas}}(\alpha_i) \right)^2} \tag{7}$$

where α_i is the set of the investigated rotation angles, and $\hat{\sigma}^j_{\mathrm{meas}}$ is the experimental error (cf. Fig. 2b). Since the relationship between the ODF and the angular dependent Raman intensity is not unambiguous if collected in only one direction, three orthogonal directions (i.e. $j = \{X, Y, Z\}$ cf. Fig. 2a) have to be evaluated. Consequently, measured data from appropriate directions have to be provided (see Eq. (7)). Since electrical poling and mechanical compression were performed along the longitudinal axis of the samples, cylindrical rotational symmetry of the domain texture was assumed here (cf. Fig. 2a), leading to a ϕ-independent distribution. Hence, measurements on only one side of the sample and suitable assumptions for the other two directions are sufficient. The present measurements were performed in the X-direction, and the data for the Y-direction were taken as $\hat{I}^Y_{\mathrm{meas}} = \hat{I}^X_{\mathrm{meas}}$ and $\hat{\sigma}^Y_{\mathrm{meas}} = \hat{\sigma}^X_{\mathrm{meas}}$. Data in the Z-direction were set to a constant value, leading after normalization to $\hat{I}^Z_{\mathrm{meas}} = 1$ and $\hat{\sigma}^Z_{\mathrm{meas}} = 0.01$ (lower bound of the experimental standard deviation). If χ^2 decreases with respect to the previous step, the new orientation vector is accepted instantly, otherwise it is accepted with a certain probability according to the Metropolis–Hastings algorithm [29]:

$$p = \exp(-\Delta\chi^2 \times \frac{n}{\tau}) \tag{8}$$

where $\Delta\chi^2$ is the deviation of χ^2 for the last two consecutive steps, and τ is the "model temperature", which is set here to $\tau = 10$. The procedure is repeated selecting a new triad at each step. The optimization routine was performed with a set of $n = 10000$ triads[2] and stopped after χ^2 reached a stable minimum. The final best fit curve is represented in Fig. 2b (solid curve), for all investigated samples. From the final set of polarization vectors, the texture ODF was derived.

In order to validate the fitting procedure with the RMC model, experimental PRS data were also fitted with the analytical approach according to Eq. (2) [18], applying the same considerations to the Raman tensor and the numerical aperture. As evident in Fig. 3, the

[1] Due to the diagonal form of the Raman tensor, the inversion of the polar axis of a triad has no influence on the Raman signal. Hence, effectively only three orientations out of six are distinguishable.

[2] Considering the grain size of the present ceramic (1. 5 μm [20]), the domain width can be estimated as 41nm [30]. The penetration depth of the used laser in PZT is 15. 3 μm (97% of the intensity signal)—as measured by preliminary defocusing experiments. This gives an estimate of ~9500 domains included within the measured Raman probe.

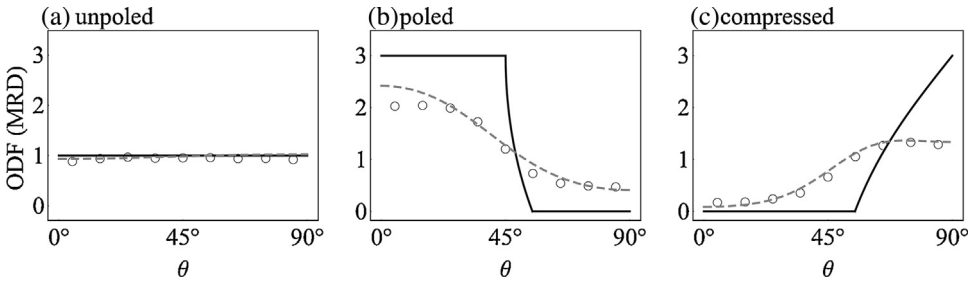

Fig. 3. ODF of the ferroelastic domains of the three investigated samples: (a) unpoled, (b) poled and (c) mechanical compressed. Each plot shows: ODF obtained from RMC fit (empty circles); ODF obtained from analytical fit with Eq. (2) (dashed grey line); ideal ODF of a saturated tetragonal domain configuration [19] (black line).

RMC fitting yields nearly the same ODF results as the analytical approach from the past literature [18] (cf. open circles and dashed grey line, respectively), with one notable exception: In the poled sample close to the poling axis, the analytically fitted ODF yields higher values than the RMC fit. Since the analytical approach used here has only two parameters, it is not possible to trace every possible distribution perfectly (as already proved in Fig. 1). The overall trend is then dominated by contributions from polar angles closer to 90°. This causes an overestimation of the domain distribution at angles close to the poling direction, an artefact that may be corrected by increasing the number of terms in Eq. (2), at the expense of increasing the complexity of calculation. Hence, the RMC model proposed here is a valid alternative to reproduce artefact-free and physically coherent ODFs from Raman data without significantly increasing computational complexity.

Comparing the measured and fitted data to the maximum theoretical ODF of each configuration [19] (i.e. unpoled, poled, compressed), it can be seen that the saturated state is not reached in the poled or in the compressed sample (cf. Fig. 3b–c). This is due to the fact that the Raman measurements were performed ex-situ in absence of applied electric field or mechanical load. Hence, only remanent and not saturated states were probed. The amount of non-permanently retained domains upon removal of electric field or mechanical load (i.e. back-switched domains) is around 20% for the poled material and up to 50% for the compressed one.

In summary, PRS measurements were conducted on differently textured PZT ceramics. By employing an RMC model to fit the angular dependent PRS data, the strain texture of each sample was obtained, and proved being in a good agreement with qualitative texture-related CGR measurements. The model was validated by comparing it with fitting performed by analytical functions, and it was proven that the RMC model can provide artefact-free results. Quantitative discrepancies to the maximum theoretical ODF for the poled and the compressed samples were mainly attributed to domain back-switching. The method detailed here can be applied to any kind of Raman-active material, provided that the Raman tensor parameters of (quasi-) single crystalline samples are available. The versatility of the RMC model opens new possibilities for texture studies by PRS.

Acknowledgements

The work was supported by the Federal Ministry for Transport, Innovation and Technology (bmvit) and Austrian Science Fund (FWF): Grant TRP 302-N20. EPCOS OHG, Deutschlandsberg (Austria), a member of the TDK-EPC Corporation, is gratefully acknowledged for providing the samples.

References

[1] G.L. Messing, S. Trolier-McKinstry, E.M. Sabolsky, C. Duran, S. Kwon, B. Brahmaroutu, P. Park, H. Yilmaz, P.W. Rehrig, K.B. Eitel, E. Suvaci, M. Seabaugh, K.S. Oh, Templated grain growth of textured piezoelectric ceramics, Crit. Rev. Solid State Mater. Sci. 29 (2004) 45–96.
[2] R. Pavlacka, R. Bermejo, Y. Chang, D.J. Green, G.L. Messing, Fracture behavior of layered alumina microstructural composites with highly textured layers, J. Am. Ceram. Soc. 96 (2013) 1577–1585.
[3] A.J. Moulson, J.M. Herbert, Electroceramics, 2nd Ed, John Wiley and Sons Ltd, West Sussex, 2003.
[4] H.G. Baerwald, Thermodynamic theory of ferroelectric ceramics, Phys. Rev. 105 (1957) 480–486.
[5] J.L. Jones, M. Hoffman, K.J. Bowman, Saturated domain switching textures and strains in ferroelastic ceramics, J. Appl. Phys. 98 (2005) 024115.
[6] Y. Saito, H. Takao, T. Tani, T. Nonoyama, K. Takatori, T. Homma, T. Nagaya, M. Nakamura, Lead-free piezoceramics, Nature 432 (2004) 84–87.
[7] M. Becker, H. Scheel, S. Christiansen, H.P. Strunk, Grain orientation, texture, and internal stress optically evaluated by micro-Raman spectroscopy, J. Appl. Phys. 101 (2007) 063531.
[8] M. Tanaka, R.J. Young, Molecular orientation distributions in uniaxially oriented poly(l -lactic acid) films determined by polarized Raman spectroscopy, J. Mater. Sci. 41 (2006) 963–991.
[9] M. Deluca, M. Higashino, G. Pezzotti, Raman tensor elements for tetragonal $BaTiO_3$ and their use for in-plane domain texture assessments, Appl. Phys. Lett. 91 (2007) 091906.
[10] J.C. Gonzalez, N. Mestres, T. Puig, J. Gazquez, F. Sandiumenge, X. Obradors, A. Usoskin, C. Jooss, H.C. Freyhardt, R. Feenstra, Biaxial texture analysis of $YBa_2Cu_3O_7$-coated conductors by micro-Raman spectroscopy, Phys. Rev. B 70 (2004) 094525.
[11] M. Asif Rafiq, P. Supancic, M. Elisabete Costa, P.M. Vilarinho, M. Deluca, Precise determination of phonon constants in lead-free monoclinic $(K_{0.5}Na_{0.5})NbO_3$ single crystals, Appl. Phys. Lett. 104 (2014) 011902.
[12] J.L. Jones, The use of diffraction in the characterization of piezoelectric materials, J. Electroceram. 19 (2007) 69–81.
[13] J.L. Jones, E.B. Slamovich, K.J. Bowman, Domain texture distributions in tetragonal lead zirconate titanate by X-ray and neutron diffraction, J. Appl. Phys. 97 (2005) 034113.
[14] T.L. Burnett, T.P. Comyn, A.J. Bell, E. Condliffe, G. Lloyd, Imaging of domains in single crystals of $BiFeO_3$-$PbTiO_3$ using various microscopy techniques, J. Phys. Conf. Ser. 26 (2006) 239.
[15] R. Loudon, The Raman effect in crystals, Adv. Phys. 13 (1964) 423–482.
[16] M. Deluca, T. Sakashita, G. Pezzotti, Polarized Raman scattering of domain structures in polycrystalline lead zirconate titanate, Appl. Phys. Lett. 90 (2007) 051919.
[17] R. Ossikovski, Q. Nguyen, G. Picardi, J. Schreiber, P. Morin, Theory and experiment of large numerical aperture objective Raman microscopy: application to the stress-tensor determination in strained cubic materials, J. Raman Spectrosc. 39 (2008) 661–672.
[18] G. Pezzotti, Raman spectroscopy of piezoelectrics, J. Appl. Phys. 113 (2013) 211301.
[19] F. Li, R. Rajapakse, Analytical saturated domain orientation textures and electromechanical properties of ferroelectric ceramics due to electric/mechanical poling, J. Appl. Phys. 101 (2007) 054110.
[20] R. Bermejo, H. Grünbichler, J. Kreith, C. Auer, Fracture resistance of a doped PZT ceramic for multilayer piezoelectric actuators: effect of mechanical load and temperature, J. Eur. Ceram. Soc. 30 (2010) 705–712.
[21] G.A. Schneider, Influence of electric field and mechanical stresses on the fracture of ferroelectrics, Annu. Rev. Mater. Res. 37 (2007) 491–538.
[22] G.R. Anstis, P. Chantikul, B.R. Lawn, D.B. Marshall, A critical evaluation of indentation techniques for measuring fracture toughness: i, direct crack measurements, J. Am. Ceram. Soc. 64 (1981) 533–538.
[23] M. Deluca, R. Bermejo, H. Grünbichler, V. Presser, R. Danzer, K.G. Nickel, Raman spectroscopy for the investigation of indentation-induced domain texturing in lead zirconate titanate piezoceramics, Scripta Mater. 63 (2010) 343–346.
[24] D. Keen, M. Tucker, M. Dove, Reverse Monte Carlo modelling of crystalline disorder, J. Phys. Condens. Matter 17 (2005) S15.
[25] R.L. McGreevy, L. Pusztai, Reverse Monte Carlo simulation: a new technique for the determination of disordered structures, Mol. Simul. 1 (1988) 359–367.
[26] M. Nakajima, T. Fujisawa, Y. Ehara, T. Yamada, H. Funakubo, H. Naganuma, S. Okamura, K. Nishida, T. Yamamoto, M. Osada, Single crystal-like selection

rules for unipolar-axis oriented tetragonal Pb(Zr, Ti)O_3 thick epitaxial films, Appl. Phys. Lett. 97 (2010) 111901.
[27] J.F. Nye, Physical Properties of Crystals. 2nd Ed., Oxford University Press, Oxford, 1985.
[28] M. Moret, M. Devillers, K. Wörhoff, P. Larsen, Optical properties of $PbTiO_3$, $PbZr_xTi_{1-x}O_3$, and $PbZrO_3$ films deposited by metalorganic chemical vapor on $SrTiO_3$, J. Appl. Phys. 92 (2002) 468–474.
[29] N. Metropolis, A.W. Rosenbluth, M.N. Rosenbluth, A.H. Teller, E. Teller, Equation of state calculations by fast computing machines, J. Chem. Phys. 21 (1953) 1087–1092.
[30] W. Cao, C.A. Randall, Grain size and domain size relations in bulk ceramic ferroelectric materials, J. Phys. Chem. Solids 57 (1996) 1499–1505.